AGMR | Hindawi

Research Article

Investigating the Impact of HTNV Infection on the Gut Microbiota of Wild-Type and NLRX1 Knockout Mice

Wenjie Sun [1,2] **Yaxin Ding** [1,2] **Ziyu Liu** [1] **Shiyuan Hou,**[1] **Danni Sun,**[1] **Ruixue Ma,**[1] **Huarui Kang,**[3] **Xiaohan Ma,**[3] **Jiayu Wang,**[3] **Hongrui Mu,**[3] **Yunhua Lv,**[1] **Tianle Gu,**[1] **Qikang Ying,**[1] **Fang Wang,**[1] **Xingan Wu** [1] **and Rongrong Liu** [1]

[1]*Department of Microbiology, School of Basic Medicine, Fourth Military Medical University, Xi'an, China*
[2]*College of Life Science, Northwest University, Xi'an, China*
[3]*School of Basic Medicine, Fourth Military Medical University, Xi'an, China*

Correspondence should be addressed to Xingan Wu; wuxingan@fmmu.edu.cn and Rongrong Liu; rong4713@163.com

It is becoming increasingly clear that maintaining the equilibrium of gut microbiota homeostasis during viral infections, such as Hantaan virus (HTNV), is of paramount importance. In order to gain insight into the role of NOD-like receptors in the immune system, we conducted a comparative study between C57BL/6 and $Nlrx1^{-/-}$ mouse models to analyze changes in the gut microbiota after HTNV infection. Our findings revealed an increase in the ratio of *Firmicutes* to *Bacteroides* in $Nlrx1^{-/-}$ mice, suggesting a potential link to inflammation. In addition, a comprehensive analysis of serum metabolomics revealed that differential metabolites were mainly concentrated in amino acid metabolism and lipid metabolism. Amino acid metabolism mainly involves arginine, lysine, and histidine metabolism, while lipid metabolism is mainly related to glycerophospholipid metabolism and fatty acid synthesis. Analysis of the correlation between microbiota and metabolites revealed an inverse relationship between Bacteroidetes and metabolites related to glutamine metabolism, while Firmicutes were directly associated with these metabolites. Furthermore, we observed a negative correlation between the presence of *Actinobacteria*, *Proteobacteria*, and *Patescibacteria* and the metabolites related to polyunsaturated fatty acids (PUFAs). Our results demonstrate that HTNV infection causes changes in the composition of gut microbiota in both $Nlrx1^{-/-}$ and wild-type (WT) mice. Moreover, the fecal microbiota and serum metabolites of $Nlrx1^{-/-}$ mice display notable differences at various developmental stages. Investigating this further may help to improve our understanding of the pathogenesis of HTNV and provide potential therapeutic options.

1. Introduction

Hantaan virus (HTNV) is a virus with single-stranded RNA and a negative sense, frequently spread by rodents through their urine, feces, saliva, and aerosols. This virus is responsible for inducing varying levels of severity in Asia and Europe, resulting in hemorrhagic fever with renal syndrome (HFRS). During an episode of HFRS, the renal vascular endothelium is primarily affected, with common symptoms including thrombocytopenia, leukocytosis, anemia, and infiltration of inflammatory cells. Recent studies have also suggested that HTNV infections can have an impact on the intestinal tract, as evidenced by the case of a 54-year-old patient with acute kidney failure caused by inflammatory diarrhea and a fourfold rise in HTNV antibody levels during the acute phase [1]. Furthermore, the homeostasis of the gut microbiota is often disturbed by virus infections, leading to alterations in its composition and activity [2, 3]. Several viruses, including SARS-CoV-2 [4–8], influenza A virus [9–11], and HIV [12–14], have been proved to affect the gut microbiota. However, there has yet to be an investigation into the changes in the gut microbiota composition and the

metabolites produced by commensal microbes after HTNV infection. To gain a better understanding of this, it is essential to examine the gut microbiota and symbiotic metabolites post-HTNV infection.

Research has shown that viral infection can affect bacterial abundance and cellular metabolism. In terms of microbial abundance, the diversity of microbial characteristics in patients with severe acute respiratory syndrome coronavirus type 2 infection has significantly decreased. It is believed that this decline in variety may be linked to the severity of the disease, as those with more severe cases of the illness seem to display signs of intestinal dysbiosis [15]. Severely infected patients have been observed to have increased numbers of harmful bacteria such as *Enterobacteriaceae* and *Desulfovibrionaceae*, accompanied by a decrease in the number of beneficial bacteria such as *Ruminococcaceae* and *Lachnospiraceae* [16]. Similarly, individuals with influenza (IAV) have been noted to exhibit similar alterations in their gut microbiota, with a decrease in the diversity of beneficial bacteria [17] .This decrease has been associated with an increased vulnerability to enteric bacterial infections [18]. Furthermore, research has shown that mice infected with IAV have a higher presence of *Enterobacteriaceae* in their respiratory systems [9]. Additionally, individuals with HIV-1 infection have been observed to have a reduction in certain advantageous microbes, such as *Bacteroides*, *Akkermansia*, *Anaerovibrio*, *Bifidobacterium*, and *Clostridium* [12]. In terms of cellular metabolism, the research by Xue et al. has shown that African swine fever virus (ASFV) infection increases host amino acid metabolism, TCA cycle, and lactate production to inhibit host innate immune response [19]. There are reports that after HIV-1 infection with CD4+T cells, glutamate secretion increases to promote the TCA cycle, induce high levels of oxidative phosphorylation, and promote HIV-1 replication [20] MCV upregulates glutamine transporter SLC1A5, glutaminase GLS, and glutamate dehydrogenase GLUD1 to promote the TCA cycle (glutamine breakdown), thereby promoting aerobic glycolysis and conversion [21]. HCV infection enhances the utilization of glutamine, which promotes the expression of key enzymes involved in glutamine degradation in a c-Myc-dependent manner. In addition, enhanced glutamine metabolism is also beneficial for the replication of hepatitis C virus [22].

The arrangement of the gut microbiota may influence the activity of pattern recognition receptors (PRRs), thereby increasing recognition of harmful bacteria and promoting the expression of proinflammatory factors, subsequent leading to inflammation and dysbiosis [23]. NLRX1, a mitochondria-associated negative regulator, has been linked to various processes such as the control of inflammation, autophagy, and mitophagy, interferon signaling, and the generation of reactive oxygen species in response to viral and bacterial pathogens. Morrison et al. found that the absence of NLRX1 can alter the composition of microorganisms, and a sustained gluten-free diet (GFD) can lead to a lack of micronutrients (short-chain fatty acids, etc.) used in microbial metabolic activities, resulting in the loss of beneficial microorganisms and an increase in the abundance of pathogenic microorganisms [24]. As NLRX1 functions as a cytosolic receptor for both host and microbe components, its effects may be pathogen-specific. However, further researches are needed to determine whether NLRX1 affects the host's antiviral response and gut microbiota after virus infection.

16S rDNA sequencing technologies allowed us to compare the differences in gut microbiota between WT and $Nlrx1^{-/-}$ C57BL/6 mice after HTNV infection. Our findings demonstrate that HTNV infection and serum metabolites had a substantial effect on the gut microbiota of both types of mice. This implies that this experimental model can be useful for interventions aimed at manipulating the gut microbiota to improve HTNV control.

2. Materials and Methods

2.1. Virus Stocks. The HTNV strain 76-118 was generously donated by the Chinese Center for Disease Control and Prevention. Our laboratory took great care in preserving and expanding the virus, using Vero E6 cells for propagation. The 50% tissue culture infectious dose (TCID50) was determined by immunofluorescence assays (IFAs). The multiplicity of infection (MOI) was defined as the number of plaques forming units (PFUs) computed as PFU = 0.7 × TCID50.

2.2. Generation of Nlrx1 Knockout Mouse Model. The Shanghai Model Organisms Center, Inc. in Shanghai, China, created two mouse models: C57BL/6J wild-type and $Nlrx1^{-/-}$. To generate the $Nlrx1^{-/-}$ mice, exons 2-3 of the NLRX1 gene were eliminated by utilizing two sgRNAs: 5′-CCAAGACAT TAGCTGCATGT-3′ and 5′-TTTGGACAGGTCGCGC GTAG-3′. C57BL/6J zygotes were injected with sgRNAs and Cas9 mRNA synthesized in vitro and then transferred to pseudopregnant mice. Primer pairs F-5′-GCAGGGCAA CAGGAAAGAAAGTGG-3′ and R-5′-GGTGGAAGGCC GGGTGGTTAC-3′ were utilized to verify the genotype of the F0 mice. Additionally, PCR and sequencing techniques were employed, and F0 mice were bred with C57BL/6J mice to acquire F1 heterozygous $Nlrx1^{-/-}$ mice. Homozygous $Nlrx1^{-/-}$ mouse was generated by intercrossing the F1 heterozygous mice. All studies were conducted using mice aged 6-8 weeks.

2.3. Animal Infection, Ethics, and Biosafety Statement. A total of 20-25 Nlrx1-/- and WT mice were administered 500,000 plaque-forming units of HTNV in 50 μL of media intraperitoneally. These mice were divided into five groups and were collected at 0-, 3-, 6-, 9-, and 12-day postinfection. For testing purposes, 8-10 animals from each group were humanely euthanized. Fresh fecal samples were collected from the mice and stored at -80°C for microbiota analysis. Additionally, blood specimens were taken from mice by removing the eyeballs, and serum samples were used for UHPLC-MS/MS. The protocol for the animal study was approved by the Fourth Military Medical University Animal Center's Committee of Laboratory Experimentation (no. 20210403). All necessary precautions were taken to ensure that the animals were kept in minimal distress and the minimum number of animals was used.

2.4. 16S Sequencing and Gut Microbiota Analysis. Research was conducted to analyze the composition of the microbiota population following HTNV infection. 50 grams of recently excreted mouse droppings was collected and preserved at -80°C using liquid nitrogen. The Magen HiPure Stool DNA Kit was employed to isolate and purify the microbial DNA. The bacterial 16S rDNA V3-V4 region was then amplified using the extracted DNA and barcode-indexed primers 341F and 806R. The Illumina platform was utilized by Guangzhou Genedenovo Biotechnology Co. to normalize, pool, and sequence the amplicons. The UCHIME algorithm is used to reject chimeric labels and cluster successful labels into operational classification units (OTUs) with a similarity threshold of 97% or higher. For each OTU, a representative sequence was selected, and the taxonomic details were annotated with the RDP classifier (version 2.2) and the SILVA database (version 132).

2.5. Untargeted Liquid Chromatography-MS Metabolomics Analysis. Samples of $100 \mu L$ were extracted using a mixture of methanol and acetonitrile ($1:1$, v/v) of $400 \mu L$. The specimens were then sonicated at 40 kHz for 30 minutes at 5°C. To precipitate proteins, the samples were kept at -20°C for 30 minutes and centrifuged at 13000g for 15 minutes at 4°C. The supernatant was transferred to new microtubes and evaporated under a nitrogen stream to dryness. For the UHPLC-MS/MS analysis, the samples were sonicated in a water bath at 5°C and reconstituted in a loading solution of acetonitrile and water ($1:1$, v/v) with a total volume of $100 \mu L$. After centrifugation at 13000 g for 15 minutes at 4°C, the supernatant was transferred to sample vials for LC-MS/MS analysis using an AB SCIEX UPLC-TripleTOF system. The raw data of LC/MS was preprocessed, and a three-dimensional data matrix in CSV format was generated using Progenesis QI software from Waters Corporation. Databases utilized for identification included HMDB, Metlin, and Majorbio databases. Through metabolic enrichment and pathway analysis via database searches, researchers identified various metabolites that differed between the two groups and associated them with their corresponding biochemical pathways.

2.6. Statistical Analysis. All statistical analyses were conducted using GraphPad Prism v6 software. For microbiota data, Welch's t-test, Wilcoxon's rank test, Tukey's HSD test, Kruskal-Wallis' H test, Adonis (also known as PERMANOVA), and ANOSIM test were performed in R project vegan package (version 2.5.3). For metabolomics data, multivariate statistical analysis was conducted using the ropls R package (version 1.6.2) from Bioconductor on the Majorbio Cloud Platform, the confidence level of PLS-DA analysis is 0.95, and the metabolite clustering tree (Figures 1(c) and 1(d)) shows the top 30 metabolites with VIP > 1. All statistical analyses were considered statistically significant if the p value was less than 0.05. Significance is represented by ∗, where ∗ represents $p < 0.05$, ∗∗ represents $p < 0.01$, and ∗∗∗ represents $p < 0.001$.

3. Results

3.1. HTNV Infection Has a Discernible Impact on α and β Diversity of the Gut Microbiota in Both WT and $Nlrx1^{-/-}$ Mice. Analysis of 16S rDNA gene amplicons revealed that out of 381 operational taxonomic units (OTUs) identified, 247 were common to both WT and $Nlrx1^{-/-}$ mice. The WT group had 51 distinct OTUs, while the $Nlrx1^{-/-}$ mouse group had 48 OTUs (Figure 2(a)). The Shannon index was used to measure the uniformity and richness of the gut microbiota, which showed a significant decrease in community richness in WT mice at 9 dpi (Figure 2(b)). On the other hand, the $Nlrx1^{-/-}$ group experienced a decrease in the Shannon index at 3 dpi. Statistical tests of the Shannon index revealed significant differences in the abundance and diversity of the gut microbiota between WT and $Nlrx1^{-/-}$ mice following HTNV infection, particularly at 3 and 12 days (Figure 2(c)).

Principal coordinate analysis of β diversity, which was conducted using UniFrac distance analysis, indicated that the microbiota of mice in the experimental group formed distinct clusters at different time point postinfection with the virus (Figure 2(d)). PCo1 (33.97%) revealed distinct separation of unweighted UniFrac distances between WT and $Nlrx1^{-/-}$ mice following HTNV infection, suggesting an impact of the virus on the β diversity of the gut microbiota in mice.

3.2. HTNV Infection Leads to a Noticeable Alteration Population of Gut Microbiota in Both WT and $Nlrx1^{-/-}$ Mice. Analysis of the gut microbiota composition at various taxonomic levels revealed changes in both α and β diversities. 16S rDNA sequencing of normal mice revealed the predominant categories at phylum to be *Firmicutes* and *Bacteroidetes*, along with smaller amounts of *Proteobacteria* and *Actinobacteria*. *Verrucomicrobia* was found in the commensal microbiota of $Nlrx1^{-/-}$ and WT mice and was particularly abundant in $Nlrx1^{-/-}$ mice. In contrast, only a small number of *Patescibacteria* were found in WT mice (Figure 3(a)). After HTNV infection, the prevalence of *Firmicutes* in WT mice rose from 42.62% to 56.44% within the first 6 days and then returned to its original level. During the course of infection in $Nlrx1^{-/-}$ mice, overall there was a 26.54% increase in the prevalence of *Firmicutes* and a corresponding decrease in *Bacteroidetes*. During the intermediate stage of infection in $Nlrx1^{-/-}$ mice (6 dpi), *Proteobacteria* and *Actinobacteria* levels increased by 3.72% and 5.46%, respectively (Figure 3(a)).

At a reduced taxonomic level (Figure 3(b)), WT mice showed an increase in *Lactobacillaceae* abundance after 9 days of infection, while *Ruminococcaceae* decreased by 8.32%. In the $Nlrx1^{-/-}$ group, *Lactobacillaceae* has a certain abundance of its own, peaking on the day 9 after infection and remains at a high level. The proportion of *Bacteroidaceae* rose to 9.80% at 3 dpi, and *Akkermansiaceae* and *Erysipelotrichaceae* both showed an increase in abundance in the later stages of infection. At the genus level (Figure 3(c)), both WT and $Nlrx1^{-/-}$ mice experienced variations in the prevalence of *Lactobacillus*, with the highest proportions of 19.65% and 33.71%, respectively, at 9 dpi. In general,
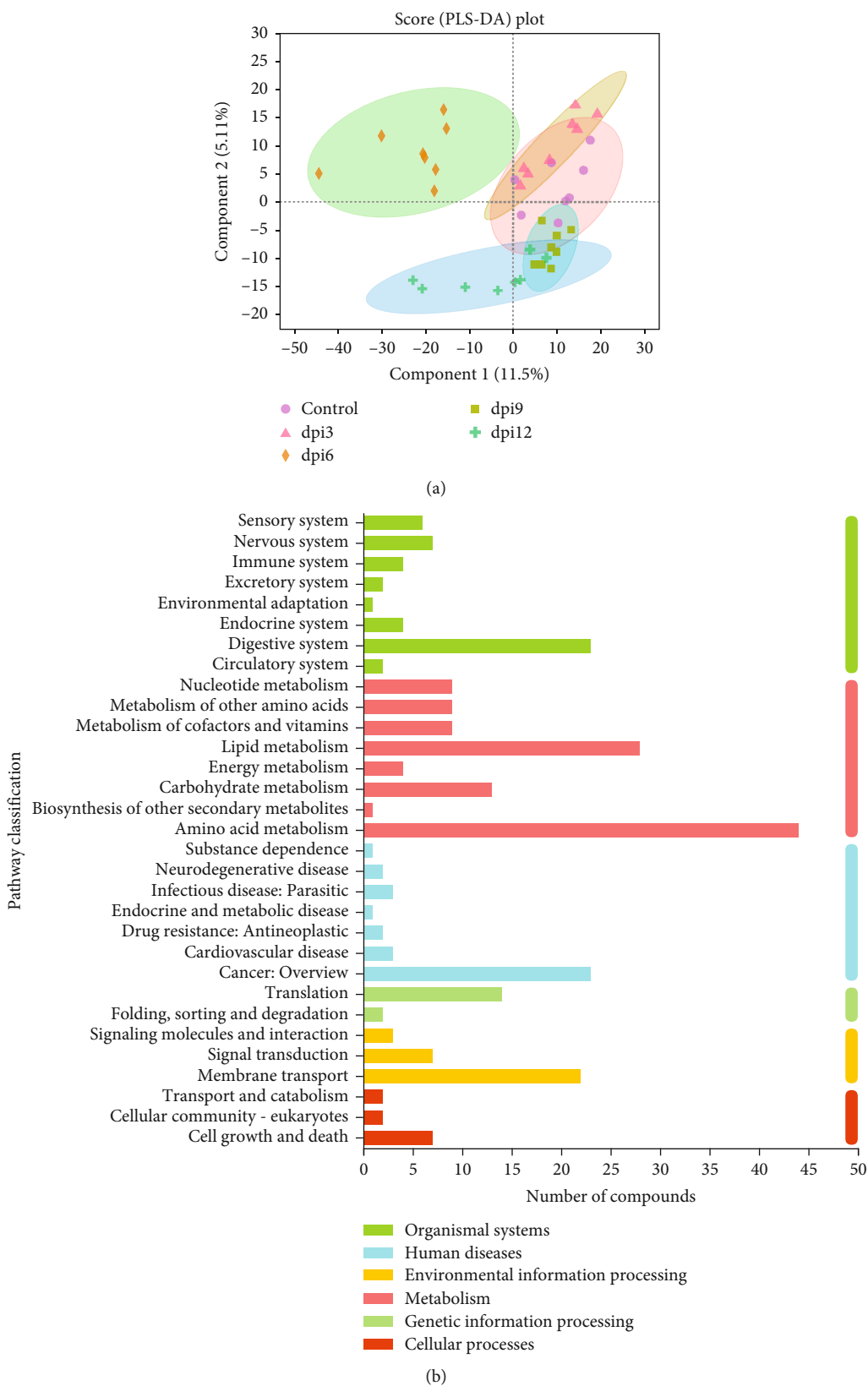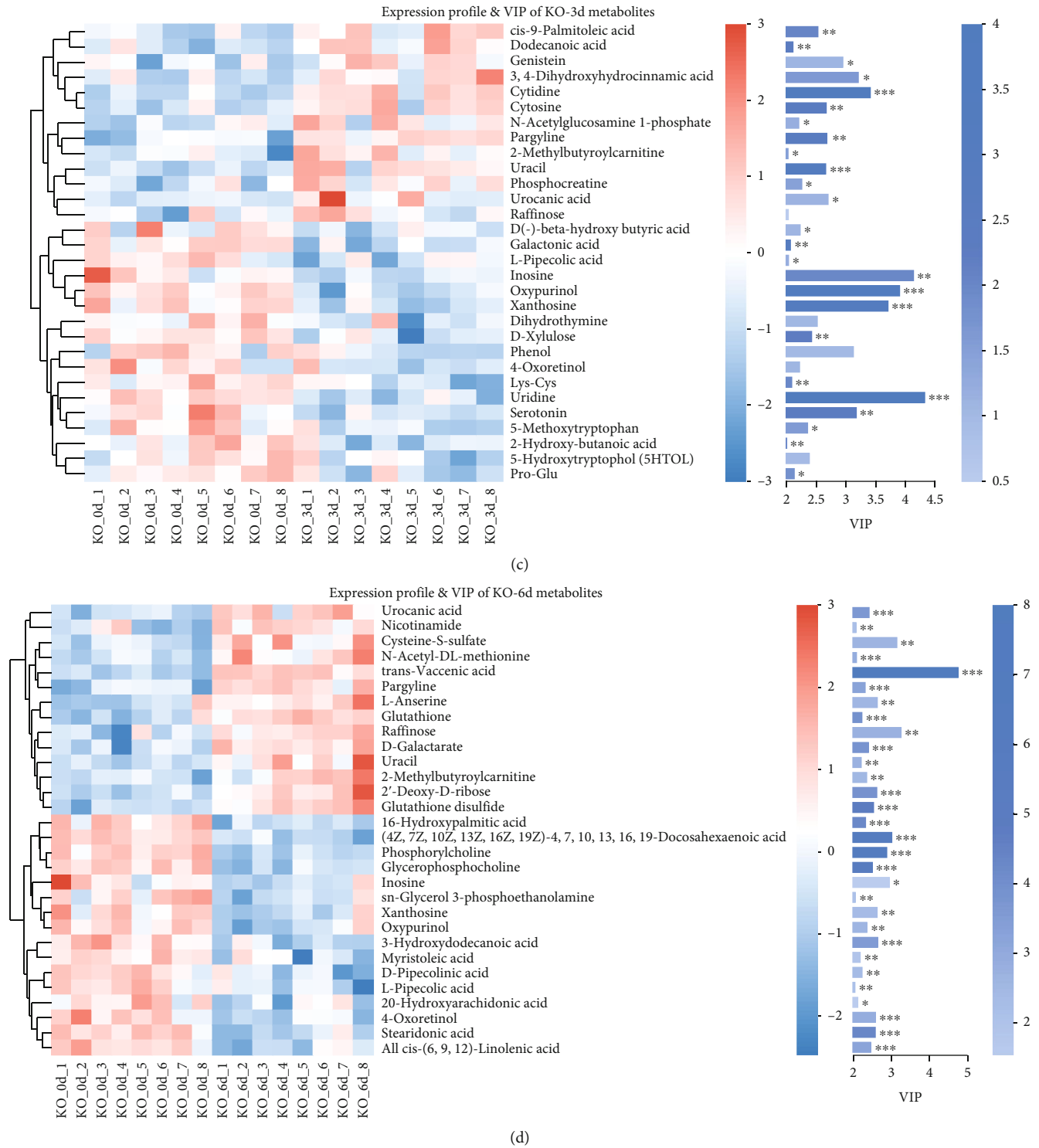
(a)

(b)

FIGURE 1: Continued.

(c)

(d)

Figure 1: HTNV infection alters metabolites in Nlrx1-/- mice. (a) Partial least square discriminant analysis (PLS-DA) models can be utilized to discriminate between control and HTNV-infected Nlrx1-/- mice. (b) The KEGG compound classification is represented by a bar graph, with the primary classification of compounds indicated by the color of the bar. (c, d) Metabolite clustering tree, the color indicates the relative expression of the metabolite in (c) 3 dpi and (d) 6 dpi.

Akkermansia was predominantly distributed in *Nlrx1⁻/⁻* mice. *Desulfovibrio* was more abundant at 12 dpi in WT mice while at 6 dpi in *Nlrx1⁻/⁻* mice. *Dubosiella* reached 17.99% during the later stages of the infection in *Nlrx1⁻/⁻* mice. In comparison to WT mice, *Nlrx1⁻/⁻* mice exhibited a

distinct trend in the relative abundance of microbiota. Notably, *Bacteroides* decreased during infection, while *Firmicutes* showed a gradual increase and reached its highest level at 12 dpi. The ratio of *Firmicutes* to *Bacteroides* in *Nlrx1⁻/⁻* mice increased. Additionally, *Nlrx1⁻/⁻* mice had elevated levels of

(a)

(b)
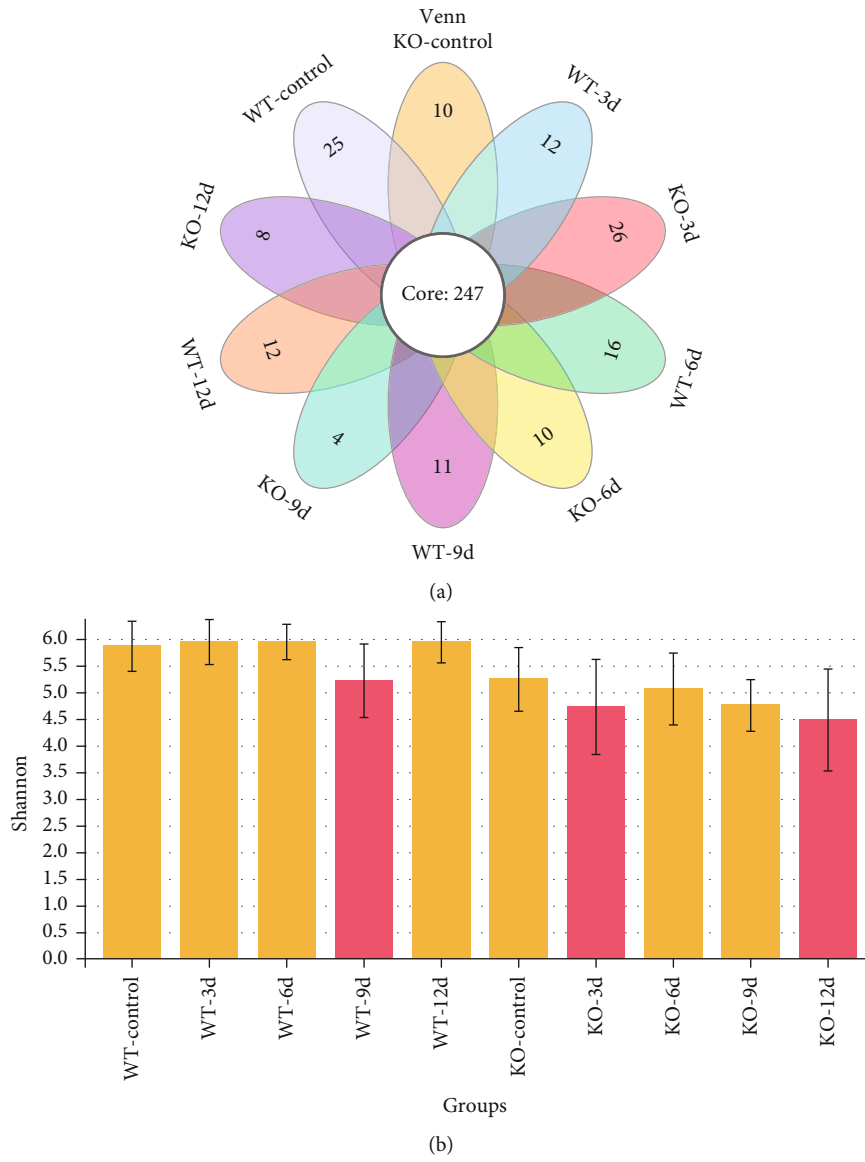
Figure 2: Continued.
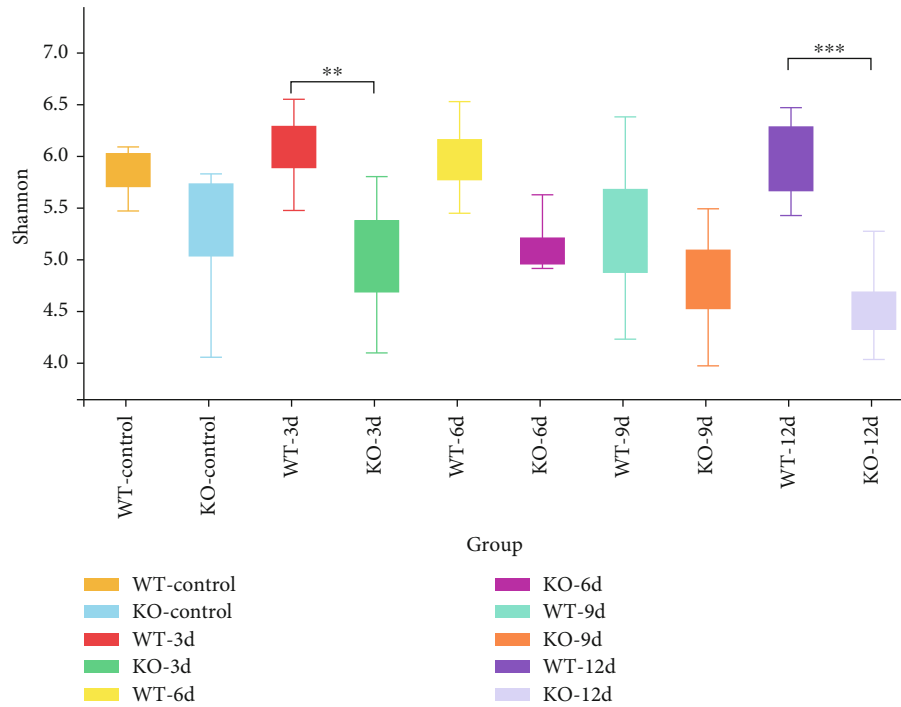
(c)
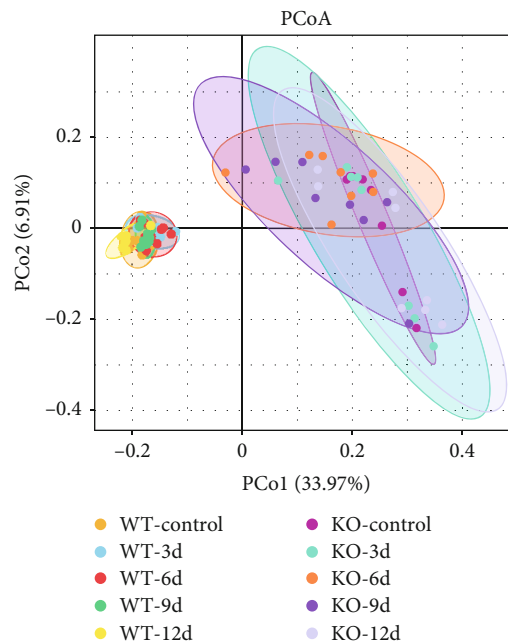
(d)

FIGURE 2: Alterations to α and β diversity of gut microbiota have been observed in both WT and *Nlrx1*$^{-/-}$ mice due to HTNV infection. (a) Among the 381 OUTs identified, 247 were determined to be core OTUs in the two groups. (b) The Shannon diversity index was used to estimate α diversity; WT: $N = 10$ at each time point; *Nlrx1*$^{-/-}$: $N = 8$ at each time point. (c) The Tukey HSD test was utilized to draw a box line diagram of the α diversity index, with a significance level of $p < 0.05$. (d) Through principal coordinate analysis (PcoA) based on unweighted UniFrac distances, β diversity was analyzed. PCo1 and PCo2 were the principal coordinates that accounted for the majority of the diversity.

Verrucomicrobia, as well as an increased prevalence of *Lactobacillaceae* in their microbial community. And there was an overall higher prevalence of *Akkermansia* compared to WT mice, while Dubosiella peaked at 12 dpi.

Based on KEGG enrichment analysis (Figure 3(d)), the functional prediction of the microbiota in WT mice mainly includes transcription, signal transduction, immune system, and cell motility. WT mice at 3 dpi and 6 dpi were also
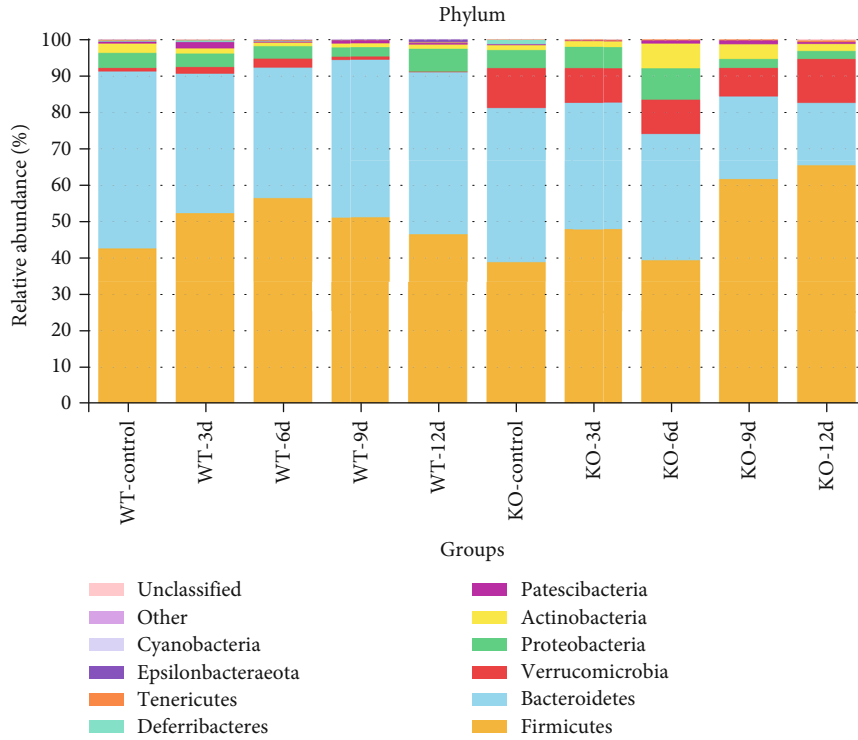
(a)
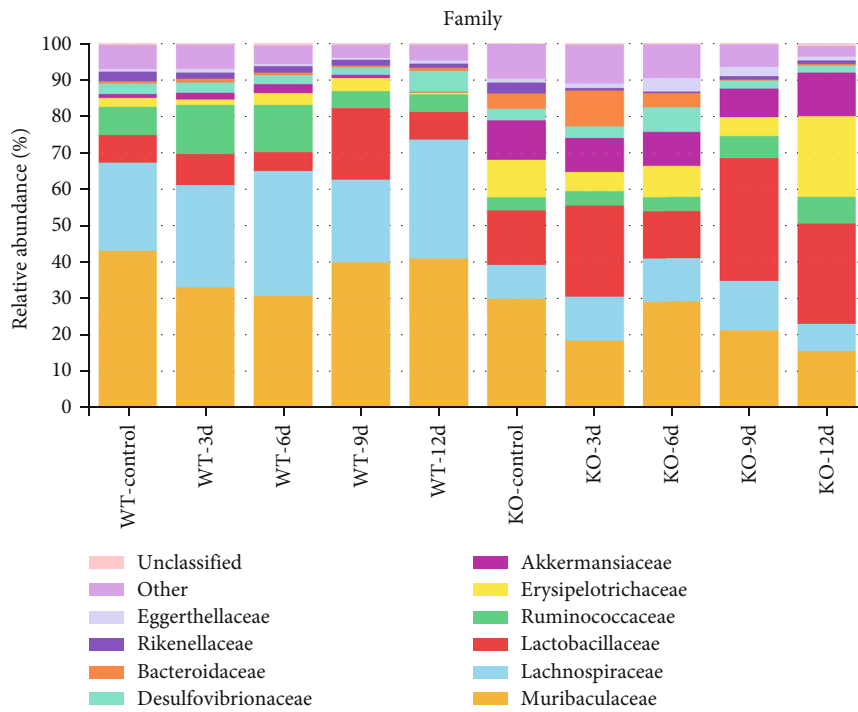
(b)

FIGURE 3: Continued.
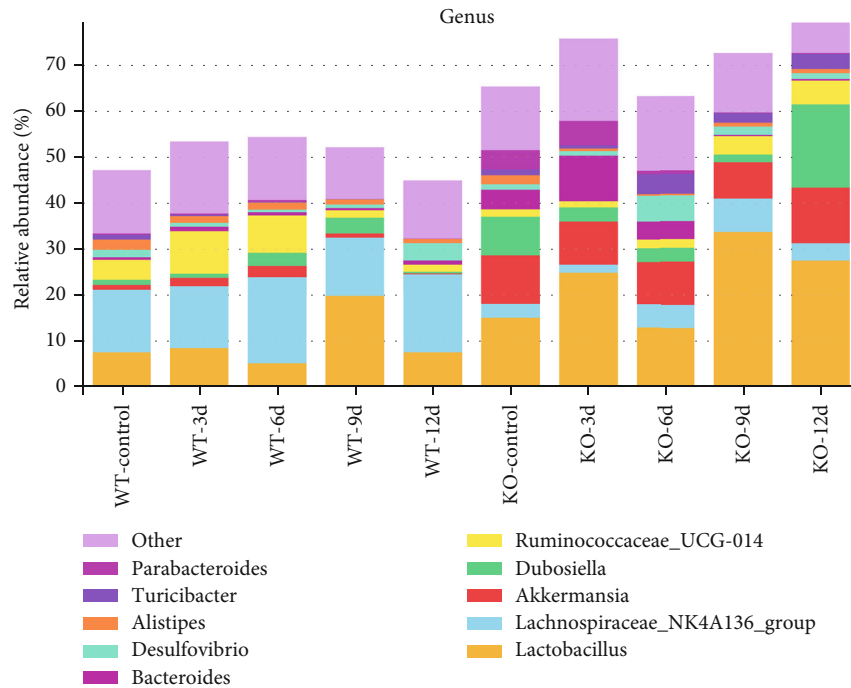
(c)
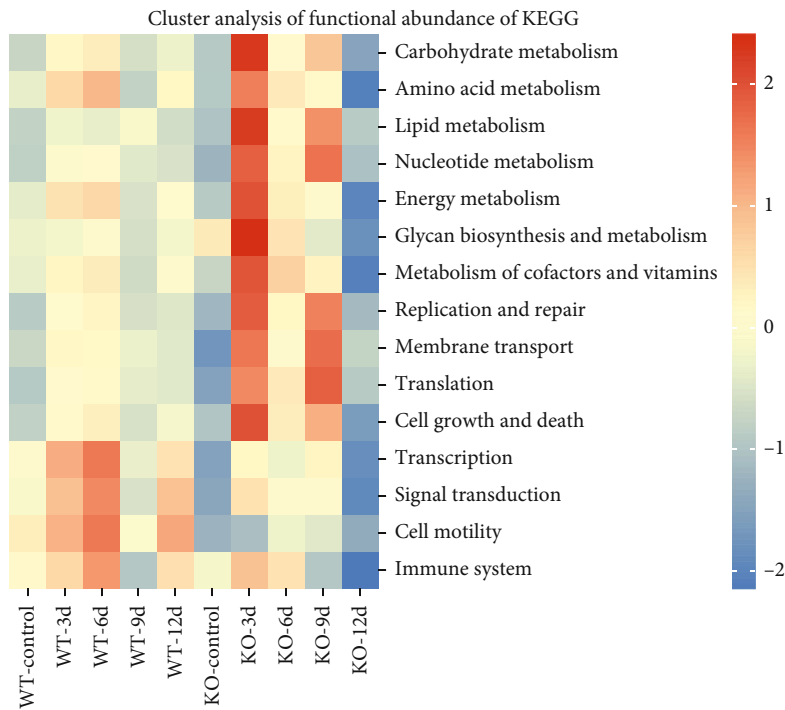
(d)

FIGURE 3: HTNV infection alters gut microbiota abundance in WT and Nlrx1-/- mice. At each time point during infection ($n = 8$), the composition of the bacterial microbiota at the (a) phylum, (b) family, and (c) class level was determined for each animal. (d) Cluster analysis of functional abundance of KEGG related to microbial communities.

involved in amino acid metabolism and lipid metabolism. However, $Nlrx1^{-/-}$ mice were mainly involved in metabolic pathways, including carbohydrate metabolism, lipid metabolism, amino acid metabolism, membrane transport, and cell growth and death.

3.3. Alterations in Plasma Metabolites of $Nlrx1^{-/-}$ Mice Infected with HTNV Were Observed. Metabolomics was used to analyze the changes in serum samples from HTNV-infected $Nlrx1^{-/-}$ mice. PLS-DA was deployed to differentiate the HTNV infection groups from the control group, as

TABLE 1: Compounds and metabolic pathways related to lipid metabolism and amino acid metabolism after 3 days of HTNV infection.

Metabolic type	Pathway description	Metabolites
Lipid metabolism	Glycerophospholipid metabolism	Phosphorylcholine
	Fatty acid biosynthesis	cis-9-Palmitoleic acid, dodecanoic acid
Amino acid metabolism	Tyrosine metabolism	3,4-Dihydroxyhydrocinnamic acid
	Arginine and proline metabolism	Phosphocreatine
	Lysine degradation	L-Pipecolic acid
	Histidine metabolism	Urocanic acid

depicted by the score plot (Figure 1(a)). The PLS-DA method had an 11.5% variance in PLS1 and 5.1% in PLS2 elements, and a clear distinction between the infected group and the uninfected group was observed ($R^2X = 0.115$, $Q^2 = 0.119$).

Analysis of 161 metabolites that were differentially expressed in $Nlrx1^{-/-}$ mice upon exposure to HTNV infection revealed that most of them were associated with amino acid metabolism and lipid metabolism (Figure 1(b)). Further, the KEGG pathways were arranged in the categories of environmental information interaction and cell process, such as membrane transport, signal transduction, cell proliferation, and death. This finding was consistent with the KEGG forecast analysis of the intestinal bacteria in $Nlrx1^{-/-}$ mice (Figure 3(d)).

Analysis of the sera from $Nlrx1^{-/-}$ mice infected with HTNV revealed a total of 161 metabolites, 81 of which were identified in positive ion mode and 80 in negative ion mode. Notable fluctuations were observed in proteins, lipids, and simple sugars. The main components in the serum samples were organic acids and their derivatives (37.59%), lipids (21.99%), and organic cyclic compounds (13.48%). At the subclass level, polypeptides and their counterparts, fatty acids and their conjugates, carbohydrates and carbohydrate conjugates, pyrimidines, purines and their derivatives, and bile acids, alcohols, and their derivatives were present in proportions of 33.33%, 11.35%, 8.51%, 4.96%, 2.84%, and 1.42%, respectively (Supplementary Figure 1).

3.4. A Comparison of the Plasma Metabolites in $Nlrx1^{-/-}$ Mice Infected with HTNV at Different Time Points Revealed Variations. An analysis of the top 30 metabolites in mouse serum revealed changes in metabolite expression during HTNV infection. During the initial phase of infection at 3 dpi, $Nlrx1^{-/-}$ mice displayed a marked increase (VIP > 2) in the levels of fatty acids and their derivatives, such as dodecanoic acid and cis-9-palmitoleic acid. Additionally, uracil and cytosine were found to be significantly elevated (VIP > 2.5), and the level of the metabolite 3,4-dihydroxychlorocinnamic acid (3,4-DHCA) produced by the hydrogenation of caffeoylquinic acid also increases, and this metabolite mainly participates in tyrosine metabolism; the levels of phosphocreatine, which participates in the metabolism of arginine and proline; L-pipecolic acid, which participates in the degradation of lysine and also increases after infection; and urocanic acid, which is involved in histidine metabolism, are downregulated after infection (Figure 1(c)).

Isoleucine was observed to rise in tandem with its partially broken down by product, ketoleucine (VIP > 1.5), which is a toxic compound in metabolism. Conversely, oxypurinol (VIP = 3.9114), serotonin (5-HT) (VIP = 3.1821), and L-leucine (VIP = 1.5676) showed significant downregulation in both the 3 dpi and 6 dpi groups.

Significant alterations in lipid metabolism were observed in mice that lacked NLRX1 after being infected with HTNV for 6 days (Figure 1(d)). Notably, the metabolites responsible for the production of polyunsaturated fatty acids (PUFAs), such as 4,7,10,13,16,19-docosahexaenoic acid (DHA), all cis-(6, 9, 12)-linolenic acid (GLA), and myristic acid, were significantly reduced. The most substantial decrease was observed in DHA. The levels of glycerophosphocholine, phosphatidylcholine, and sn-glycerol-3-phosphateethanolamine involved in the metabolism of glycerophospholipids also decreased. L-Pipecolic acid, which participates in amino acid metabolism, is downregulated, while uric acid, L-serine, and cysteine S-sulfate are upregulated. In addition, glutathione (GSH) is the major intracellular antioxidant in the liver. It is present in both reduced (GSH) and oxidized (glutathione disulfide (GSSG)) in $Nlrx1^{-/-}$ mice at 6 dpi.

Finally, we summarize the metabolic pathways involved in lipid and amino acid metabolites of HTNV infection for 3 and 6 days in Tables 1 and 2, respectively.

3.5. Nlrx1$^{-/-}$ Mice Post-HTNV Infection Were Investigated for the Association between the Fecal Microbiome and Serum Metabolites. The LEfSe method, based on linear discriminant analysis (LDA), was used to differentiate microbial communities in $Nlrx1^{-/-}$ mice at different stages of HTNV infection (Figure 4(a)). This analysis revealed that Bacteroides and Parabacteroides were the primary inhabitants in the intestines of $Nlrx1^{-/-}$ mice at 3 dpi. However, at 6 dpi and 9 dpi, Actinobacteria (Bifidobacterium, Enterorhabdus, and Coriobacterium), Proteobacteria (Desulfovibrio), and Firmicutes (Turicibacter) became more dominant. At 12 dpi, Firmicutes (Lactobacillus, Dubosiella, and Ruminococcaceas-UCG-014) were the predominant bacteria in the gut, along with the emergence of potentially harmful bacteria such as Erysipelotrichaceae in Tenericutes, which suggests the possibility of intestinal damage.

An investigation of the correlation between distinct microbiota and metabolites in $Nlrx1^{-/-}$ mice after HTNV infection is presented in Figure 4(b). The Spearman correlation coefficients of the serum showed a negative correlation between Bacteroidetes and glutamine metabolic metabolites

TABLE 2: Compounds and metabolic pathways related to lipid metabolism and amino acid metabolism after 6 days of HTNV infection.

Metabolic type	Pathway description	Metabolites
Lipid metabolism	Glycerophospholipid metabolism	Glycerophosphocholine, phosphorylcholine, sn-glycerol 3-phosphoethanolamine
	Biosynthesis of unsaturated fatty acids	(4Z,7Z,10Z,13Z,16Z,19Z)-4,7,10,13,1 6,19-Docosahexaenoic acid, all cis-(6,9,12)-linolenic acid
	Ether lipid metabolism	Glycerophosphocholine, sn-glycerol 3-phosphoethanolamine
	Linoleic acid metabolism	all cis-(6,9,12)-Linolenic acid
	Fatty acid biosynthesis	Myristic acid
Amino acid metabolism	Lysine degradation	L-Pipecolic acid
	Histidine metabolism	Urocanic acid, L-anserine
	Cysteine and methionine metabolism	Cysteine-S-sulfate

(L-glutamine and L-pyroglutamic acid), whereas *Firmicutes* positively correlated with these metabolites. *Tenericutes* were parallel with Firmicutes, which also had significantly positive correlation with glutamine metabolic metabolites. Besides, *Tenericutes* were positively correlated with L-leucine. Additionally, *Actinobacteria*, *Proteobacteria*, and *Patescibacteria* exhibited a negative correlation with metabolites related to the production of PUFAs (such as DHA, GLA, and dodecanoic acid) and bile acid metabolism, specifically GPC.

4. Discussion

The initial study of the microbiome data demonstrated that infection with HTNV influenced the composition of gut microbiota in both WT and $Nlrx1^{-/-}$ mice. The systemic immune response of the host was found to be a major factor influencing the dynamics of the gut microbiota in mice. Analysis of the data showed that HTNV infection had a significant impact both on α and β diversity in WT and $Nlrx1^{-/-}$ mice. Notably, the prevalence of harmful bacterial species such as *Desulfovibrio*, *Dubosiella*, and *Enterorhabdus* was increased in both WT and $Nlrx1^{-/-}$ mice. Furthermore, WT mice displayed an increase in the abundance of *Ruminococcaceae* during the initial 0-6 days of infection, whereas $Nlrx1^{-/-}$ mice had increased numbers of *Desulfovibrio*. Additionally, $Nlrx1^{-/-}$ mice exhibited higher levels of *Bacteroides* and *Parabacteroides* during the initial stages of HTNV infection. Moreover, in the later phase of HTNV infection (12 dpi), there was a decrease both in the presence of *Akkermansia* and *Erysipelotrichaceae* in WT mice, while $Nlrx1^{-/-}$ mice showed the opposite trend. Studies have revealed that short-chain fatty acids (SCFAs) play a crucial role in generating energy, maintaining the integrity of the epithelial barrier, and regulating the interactions between the host and gut microbiota. The microbiome data of WT mice showed an enrichment of *Ruminococcaceae* and *Prevotellaceae-UCG-014* six days after HTNV infection. The *Ruminococcaceae* family is known for its ability to generate both acetate and butyrate, which are thought to provide potential benefits in the context of viral infections. The families *Lachnospiraceae* and *Erysipelotrichaceae* have been shown to contribute to elevated levels of butyrate production, which serves as a marker for improved gastrointestinal well-being [25]. Ace-

tate and butyrate have been shown to regulate the activity of immune cells, both inside and outside the intestines, including regulatory T cells and macrophages [26, 27]. *Proteobacteria* in the gastrointestinal tract is now known to be a potential pathogen capable of causing serious illnesses in individuals with weakened immune systems [28].

Increased levels of SCFA can induce the production of NLR, which in turn suppresses inflammation [29]. After 12 days of HTNV infection, the microbiota of $Nlrx1^{-/-}$ mice was found to be composed mainly of *Firmicutes* (particularly *Turicibacter*, *Lactobacillus*, and *Dubosiella*), *Actinobacteria* (including *Bifidobacterium* and *Enterorhabdus*), and *Proteobacterial* (specifically *Desulfovibrio*) species. Meanwhile, with the decrease of *Bacteroidetes* count, the ratio of *Firmicutes* to *Bacteroidetes* in $Nlrx1^{-/-}$ mice yielded a significant increase. The *Firmicutes/Bacteroidetes* (F/B) ratio is widely accepted to have an important influence in maintaining normal intestinal homeostasis [30, 31]. A change in the F/B ratio by itself may be important since it can influence the processing of dietary polysaccharides. Pahwa et al. [32] reported that F/B ratio was restored in the NLRP3-KO mice. Except that, another research demonstrated that inhibition of NLRP3 inflammasome by administration of MCC950 to inflammatory bowel disease (IBD) mice increases the F/B ratio, which may regulate the abundance of intestinal flora and maintain intestinal homeostasis [33]. Presence of *Enterorhabdus* increases risk of bacterial infection and gastrointestinal inflammation [34].

Analysis of metabolites in the serum samples of $Nlrx1^{-/-}$ mice after HTNV infection revealed distinct changes in amino acid and lipid metabolism-related products. Lipids, as the structural basis of viruses and cells, play a central role in viral infection, influencing lipid molecules such as cholesterol and sphingolipids to selectively inhibit virus replication [35]. Peng Wei Yu et al. have shown that plant-derived natural product epiallocatechin-3-gallate (EGCG) can alleviate porcine reproductive and respiratory syndrome virus (PRRSV) infection by inhibiting lipid synthesis and autophagy [36]. Stoyanova et al. have shown that ZIKV triggers autophagy through host lipid metabolism to promote viral replication [37]. Yan et al. analyzed the lipid changes after infection with viruses such as enterovirus A71 and coxsackievirus and found that various lipids such as arachidonic

Legend:

- KO-12d
- KO-3d
- KO-6d
- KO-9d
- KO-control
- WT-3d
- WT-6d
- WT-control
- a: Bifidobacterium
- b: Bifidobacteriaceae
- c: Bifidobacteriales
- d: Actinobacteria
- e: Enterorhabdus
- f: Eggerthellaceae
- g: Coriobacteriales
- h: Coriobacteriia
- i: Bacteroides
- j: Bacteroidaceae
- k: Muribaculaceae
- l: Alistipes
- m: Rikenellaceae
- n: Parabacteroides
- o: Tannerellaceae
- p: Bacteroidales
- q: Bacteroidia
- r: Lactobacillus
- s: Lactobacillaceae
- t: Lactobacillales
- u: Bacilli
- v: Blautia
- w: Lachnoclostridium
- x: Lachnospiraceae_NK4A136_group
- y: Lachnospiraceae
- z: Ruminococcaceae_UCG_014
- a0: Ruminococcaceae
- a1: Clostridiales
- a2: Clostridia
- a3: Dubosiella
- a4: Turicibacter
- a5: Erysipelotrichaceae
- a6: Erysipelotrichales
- a7: Erysipelotrichia
- a8: Desulfovibrio
- a9: Gammaproteobacteria
- b0: Akkermansia
- b1: Akkermansiaceae
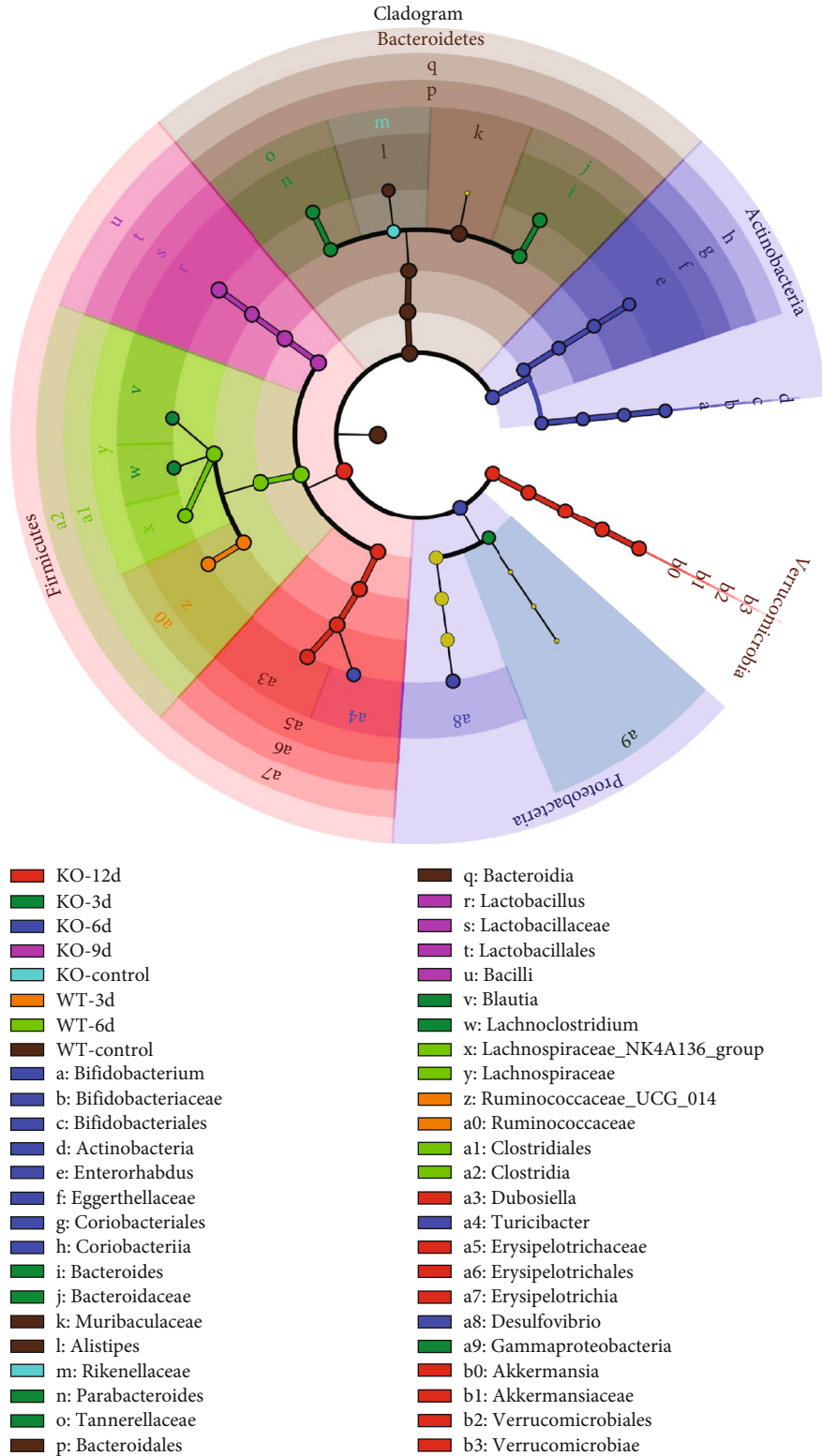- b2: Verrucomicrobiales
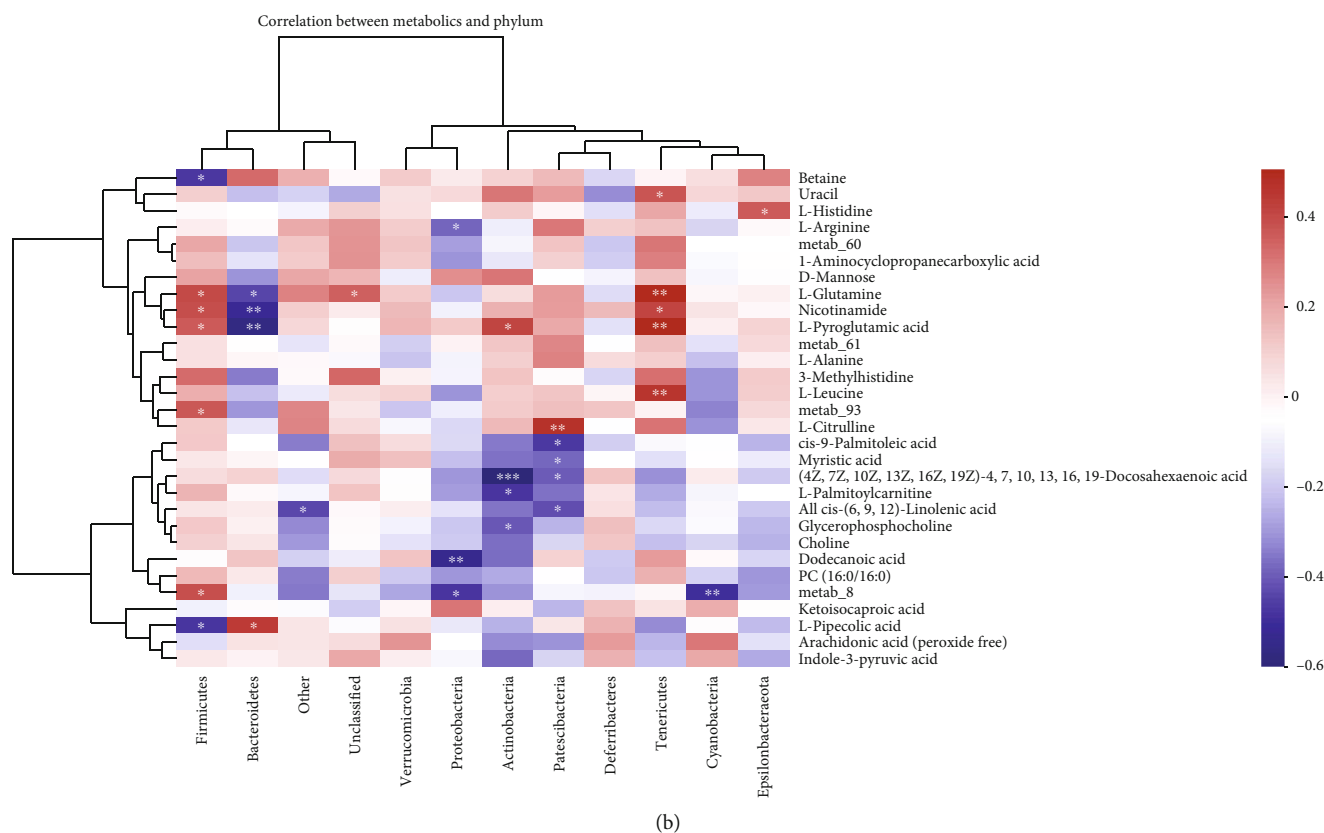- b3: Verrucomicrobiae

(a)

Figure 4: Continued.

FIGURE 4: Correlation analysis of differential microbiota and metabolites in Nlrx1-/- mice after HTNV infection. (a) Linear discriminative analysis (LDA) effect size (LEfSe) analysis. (b) Correlation analysis between sample metabolites and microbiota relative abundance at the phylum. Each grid represents the correlation between two attributes (metabolites and microorganisms), and different colors represent the correlation coefficient between them.

acid, docosahexaenoic acid, and eicosapentaenoic acid were upregulated after infection [38]. It is worth noting that lipid metabolism-related products increase after 3 days of HTNV infection and then show a decreasing trend after 6 days of infection. In addition, after 6 days of HTNV infection, the levels of PUFA and glycerophospholipids decreased, indicating a possible reduction in energy production associated with disease progression. Omega-3 PUFAs, such as DHA and eicosapentaenoic acid (EPA), are known to reduce inflammation by promoting the synthesis of anti-inflammatory eicosanoids and SPMs, such as resolvins, maresins, and protectins [39, 40]. Thus, mice with low levels of unsaturated fatty acids due to HTNV infection would be more prone to an exacerbated inflammatory response. However, further research is needed to investigate the changes and roles of lipids in the process of HTNV infection.

HTNV infection also leads to changes in amino acid levels. We found that the levels of glutamine and pyroglutamate were higher in HTNV-infected $Nlrx1^{-/-}$ mice over a 12-day period. Studies in rats have suggested that inflammation is linked to an increased hepatic glutamine transport, which is essential for cellular energy via the glutamine metabolic pathway. Correlation analysis showed that Firmicutes were positively correlated with glutamine metabolites, while Bacteroidetes were negatively correlated with them. Perna et al. showed that glutamine affects the gut microbiota

through different mechanisms, including decreasing the F/B ratio and activating the NF-κB and PI3-Akt pathways, which increases the production of endocrine immune cells in the intestinal lumen [41]. Additionally, HCV alters metabolism by increasing the consumption of glutamine, which is necessary for the virus's replication [22]. It has been reported that viral replication in EV71-infected Vero cells was augmented by glutamine, indicating that changes in the metabolism of glutamine and glutamate are critical for viral infection [42]. Besides, our results indicated that DHCA enriched in $Nlrx1^{-/-}$ mice at 3 dpi, and it is a metabolite of hydrogenation of caffeoylquinic acid with a variety of beneficial biological effects, including antiviral effects. Ogawa et al. [43] once demonstrated that DHCA inhibited severe fever with thrombocytopenia syndrome virus (SFTSV) infection in a dose-dependent manner. However, a decreased GSH/GSSG plasma ratio might reflect oxidative stress at 6 dpi in $Nlrx1^{-/-}$ mice [44, 45]. In addition, studies have shown that arginine is a direct precursor of nitric oxide (NO), which can not only act as a vasodilator and nutrient metabolism regulator but also inhibit pathogens [46]. After 3 days of HTNV infection, phosphocreatine, which is involved in arginine metabolism, is upregulated. There are reports that urocanic acid, as a UV photosensitizer, has immunosuppressive function, while urocanic acid, which is involved in histidine metabolism, is upregulated 3 days after HTNV infection and decreases 6 days later [47, 48].

Our research was the first to investigate the changes in gut microbiota and serum differential metabolites caused by HTNV infection in both WT and $Nlrx1^{-/-}$ mice. Our findings illustrated a correlation between HNTV infection and gut microbiome and metabolites. Further researches are required to uncover the exact mechanisms behind the association between HTNV infection and gut microbiota as well as metabolites in mice. In conclusion, our study revealed that HTNV infection significantly influenced the gut microbiota and serum metabolites in both WT and $Nlrx1^{-/-}$ mice.

5. Conclusions

Our study showed that HTNV infection was related to regulation of α and β diversity in the gut microbiota between WT and $Nlrx1^{-/-}$ mice. $Nlrx1^{-/-}$ mice had higher microbiota abundance than WT. Overall, three main alternations upon viral infection are as follows: (i) an increase in *Firmicutes* abundance, including the genus *Dubosiella*, especially in $Nlrx1^{-/-}$ mice, (ii) a decrease in *Bacteroidetes* abundance, and (iii) an increase in Proteobacteria abundance. On the other hand, analysis of differentially expressed metabolites in $Nlrx1^{-/-}$ mice after HTNV infection revealed that most of them were related to lipid metabolism and amino acid metabolism. Our study addresses an important research gap on the effects of HTNV infection on gut microbiota, which has not been previously explored. However, this study was a basic analysis of the gut microbiota and serum metabolites in both WT and $Nlrx1^{-/-}$ mice, and we would follow up with better designed experiments to explore and study the differential microbiota and metabolites identified in this study in more depth.

Data Availability

The sequence data discussed in this paper have been stored in the Genome Sequence Archive [28] at the National Genomics Data Center [29], which is part of the China National Center for Bioinformation/Beijing Institute of Genomics, Chinese Academy of Sciences (GSA CRA009706). These data are open to the public for access.

Conflicts of Interest

The authors declare no conflict of interest.

Authors' Contributions

R.L. and W.S. designed the study. W.S., Y.D., and Y.L. performed mouse sample collection, metabolomics, and all statistical analysis. Z.L., R.M., D.S., and S.H. were primarily responsible for methodology. H.K., X.M., J.W., and H.M. were responsible for raising BALB/C mice. T.G., Q.Y., and F.W. contributed to validation and supervision. W.S., Y.D., and Z.L. wrote the original manuscript. R.L. and X.W. did the review and supervision work, and all authors revised and approved the manuscript. Wenjie Sun, Yaxin Ding, and Ziyu Liu contributed equally to this work.

Supplementary Materials

Analysis of metabolite occupancy in serum samples from $Nlrx1^{-/-}$ mice at different classification levels using the HMDB database. Supplementary Figure 1: (a, b) compound classification of metabolites in serum samples at (a) subclass and (b) superclass levels. *(Supplementary Materials)*

References

[1] H. K. Kim, J.-H. Chung, D.-M. Kim, N.-R. Yun, C.-M. Kim, and S. Jalal, "Hemorrhagic fever with renal syndrome as a cause of acute diarrhea," *The American Journal of Tropical Medicine and Hygiene*, vol. 100, no. 5, pp. 1236–1239, 2019.

[2] J. C. Clemente, L. K. Ursell, L. W. Parfrey, and R. Knight, "The impact of the gut microbiota on human health: an integrative view," *Cell*, vol. 148, no. 6, pp. 1258–1270, 2012.

[3] N. Qin, B. Zheng, J. Yao et al., "Influence of H7N9 virus infection and associated treatment on human gut microbiota," *Scientific Reports*, vol. 5, no. 1, p. 14771, 2015.

[4] T. F. D. Liu, E. Philippou, O. Kolokotroni, G. Siakallis, K. Rahima, and C. Constantinou, "Gut and airway microbiota and their role in COVID-19 infection and pathogenesis: a scoping review," *Infection*, vol. 50, no. 4, pp. 815–847, 2022.

[5] D. Schult, S. Reitmeier, P. Koyumdzhieva et al., "Gut bacterial dysbiosis and instability is associated with the onset of complications and mortality in COVID-19," *Gut Microbes*, vol. 14, no. 1, article 2031840, 2022.

[6] Y. Liu, D. Kuang, D. Li et al., "Roles of the gut microbiota in severe SARS-CoV-2 infection," *Cytokine & Growth Factor Reviews*, vol. 63, pp. 98–107, 2022.

[7] Q. Liu, J. W. Y. Mak, Q. Su et al., "Gut microbiota dynamics in a prospective cohort of patients with post-acute COVID-19 syndrome," *Gut*, vol. 71, no. 3, pp. 544–552, 2022.

[8] T. Zuo, Q. Liu, F. Zhang et al., "Depicting SARS-CoV-2 faecal viral activity in association with gut microbiota composition in patients with COVID-19," *Gut*, vol. 70, no. 2, article gutjnl-2020-322294, 2020.

[9] S. Yildiz, B. Mazel-Sanchez, M. Kandasamy, B. Manicassamy, and M. Schmolke, "Influenza A virus infection impacts systemic microbiota dynamics and causes quantitative enteric dysbiosis," *Microbiome*, vol. 6, no. 1, p. 9, 2018.

[10] V. Sencio, A. Barthelemy, L. P. Tavares et al., "Gut dysbiosis during influenza contributes to pulmonary pneumococcal superinfection through altered short-chain fatty acid production," *Cell Reports*, vol. 30, no. 9, pp. 2934–2947.e6, 2020.

[11] K. C. Bradley, K. Finsterbusch, D. Schnepf et al., "Microbiota-driven tonic interferon signals in lung stromal cells protect from influenza virus infection," *Cell Reports*, vol. 28, no. 1, pp. 245–256.e4, 2019.

[12] M. Rocafort, M. Noguera-Julian, J. Rivera et al., "Evolution of the gut microbiome following acute HIV-1 infection," *Microbiome*, vol. 7, no. 1, p. 73, 2019.

[13] Y. Guillén, M. Noguera-Julian, J. Rivera et al., "Low nadir CD4 + T-cell counts predict gut dysbiosis in HIV-1 infection," *Mucosal Immunology*, vol. 12, no. 1, pp. 232–246, 2019.

[14] E. Yamada, C. G. Martin, N. Moreno-Huizar et al., "Intestinal microbial communities and *Holdemanella* isolated from HIV+/− men who have sex with men increase frequencies of lamina propria CCR5 $^+$ CD4 $^+$ T cells," *Gut Microbes*, vol. 13, no. 1, article 1997292, 2021.

[15] Y. K. Yeoh, T. Zuo, G. C.-Y. Lui et al., "Gut microbiota composition reflects disease severity and dysfunctional immune responses in patients with COVID-19," *Gut*, vol. 70, no. 4, pp. 698–706, 2021.

[16] T. Zuo, F. Zhang, G. C. Y. Lui et al., "Alterations in gut microbiota of patients with COVID-19 during time of hospitalization," *Gastroenterology*, vol. 159, no. 3, pp. 944–955.e8, 2020.

[17] V. Sencio, M. G. Machado, and F. Trottein, "The lung–gut axis during viral respiratory infections: the impact of gut dysbiosis on secondary disease outcomes," *Mucosal Immunology*, vol. 14, no. 2, pp. 296–304, 2021.

[18] C. A. Woodall, L. J. McGeoch, A. D. Hay, and A. Hammond, "Respiratory tract infections and gut microbiome modifications: a systematic review," *PLoS One*, vol. 17, no. 1, article e0262057, 2022.

[19] Q. Xue, H. Liu, Z. Zhu et al., "African swine fever virus regulates host energy and amino acid metabolism to promote viral replication," *Journal of Virology*, vol. 96, no. 4, article e0191921, 2022.

[20] A. Hegedus, M. K. Williamson, M. B. Khan et al., "Evidence for altered glutamine metabolism in human immunodeficiency virus type 1 infected primary human CD4+ T cells," *AIDS research and human retroviruses*, vol. 33, no. 12, pp. 1236–1247, 2017.

[21] C. Berrios, M. Padi, M. A. Keibler et al., "Merkel cell polyomavirus small T antigen promotes pro-glycolytic metabolic perturbations required for transformation," *PLoS Pathogens*, vol. 12, no. 11, article e1006020, 2016.

[22] P. L. Lévy, S. Duponchel, H. Eischeid et al., "Hepatitis C virus infection triggers a tumor-like glutamine metabolism," *Hepatology*, vol. 65, no. 3, pp. 789–803, 2017.

[23] W. Zhang, B. Tan, J. Deng et al., "PRR-mediated immune response and intestinal flora profile in soybean meal-induced enteritis of pearl gentian groupers, Epinephelus fuscoguttatus♀ × Epinephelus lanceolatus♂," *Frontiers in Immunology*, vol. 13, article 814479, 2022.

[24] H. A. Morrison, Y. Liu, K. Eden, M. A. Nagai-Singer, P. A. Wade, and I. C. Allen, "NLRX1 deficiency alters the gut microbiome and is further exacerbated by adherence to a gluten-free diet," *Frontiers in Immunology*, vol. 13, article 882521, 2022.

[25] N. Mohan and A. Sunder, "Chapter 5- From symbiosis to dysbiosis in gut-consequence includes metabolic syndrome," in *Microbial Biofilms*, H. Sarma, S. Joshi, D. Lahiri, R. R. Ray, and M. Davoodbasha, Eds., pp. 61–83, Academic Press, 2023.

[26] K. Atarashi, T. Tanoue, K. Oshima et al., "Treg induction by a rationally selected mixture of clostridia strains from the human microbiota," *Nature*, vol. 500, no. 7461, pp. 232–236, 2013.

[27] A. Hayashi, T. Sato, N. Kamada et al., "A single strain of Clostridium butyricum induces intestinal IL-10-producing macrophages to suppress acute experimental colitis in mice," *Cell Host & Microbe*, vol. 13, no. 6, pp. 711–722, 2013.

[28] R. Saito, S. Nonaka, H. Nishiyama, and N. Okamura, "Molecular mechanism of macrolide–lincosamide resistance in Mor-

[29] axella catarrhalis," *Journal of Medical Microbiology*, vol. 61, no. 10, pp. 1435–1438, 2012.

Y. D. Bhutia and V. Ganapathy, "Short, but smart: SCFAs train T cells in the gut to fight autoimmunity in the brain," *Immunity*, vol. 43, no. 4, pp. 629–631, 2015.

[30] S. Stojanov, A. Berlec, and B. Štrukelj, "The influence of probiotics on the Firmicutes/Bacteroidetes ratio in the treatment of obesity and inflammatory bowel disease," *Microorganisms*, vol. 8, no. 11, p. 1715, 2020.

[31] F. De Luca and Y. Shoenfeld, "The microbiome in autoimmune diseases," *Clinical and Experimental Immunology*, vol. 195, no. 1, pp. 74–85, 2019.

[32] R. Pahwa, M. Balderas, I. Jialal, X. Chen, R. A. Luna, and S. Devaraj, "Gut microbiome and inflammation: a study of diabetic inflammasome-knockout mice," *Journal Diabetes Research*, vol. 2017, article 6519785, pp. 1–5, 2017.

[33] S.-L. Wang, M.-M. Zhang, H. Zhou et al., "Inhibition of NLRP3 attenuates sodium dextran sulfate-induced inflammatory bowel disease through gut microbiota regulation," *Biomedical Journal*, vol. 46, no. 5, article 100580, 2023.

[34] M. Derrien, M. C. Collado, K. Ben-Amor, S. Salminen, and W. M. de Vos, "The mucin degrader *Akkermansia muciniphila* is an abundant resident of the human intestinal tract," *Applied and Environmental Microbiology*, vol. 74, no. 5, pp. 1646–1648, 2008.

[35] M. Lorizate and H. G. Kräusslich, "Role of lipids in virus replication," *Cold Spring Harbor Perspectives in Biology*, vol. 3, no. 10, article a004820, 2011.

[36] P.-W. Yu, P.-F. Fu, L. Zeng et al., "EGCG restricts PRRSV proliferation by disturbing lipid metabolism," *Microbiology Spectrum*, vol. 10, no. 2, article e0227621, 2022.

[37] G. Stoyanova, S. Jabeen, J. Landazuri Vinueza, S. Ghosh Roy, R. A. Lockshin, and Z. Zakeri, "Zika virus triggers autophagy to exploit host lipid metabolism and drive viral replication," *Cell Communication and Signaling*, vol. 21, no. 1, p. 114, 2023.

[38] B. Yan, Z. Zou, H. Chu et al., "Lipidomic profiling reveals significant perturbations of intracellular lipid homeostasis in enterovirus-infected cells," *International Journal of Molecular Sciences*, vol. 20, no. 23, p. 5952, 2019.

[39] N. Chiang and C. N. Serhan, "Specialized pro-resolving mediator network: an update on production and actions," *Essays in Biochemistry*, vol. 64, no. 3, pp. 443–462, 2020.

[40] P. Singer and P. C. Calder, "The role of omega-3 polyunsaturated fatty acids in the intensive care unit," *Current Opinion in Clinical Nutrition and Metabolic Care*, vol. 26, no. 2, pp. 129–137, 2023.

[41] S. Perna, T. A. Alalwan, Z. Alaali et al., "The role of glutamine in the complex interaction between gut microbiota and health: a narrative review," *International Journal of Molecular Sciences*, vol. 20, no. 20, p. 5232, 2019.

[42] M.-L. Cheng, K.-Y. Chien, C.-H. Lai, G.-J. Li, J.-F. Lin, and H.-Y. Ho, "Metabolic reprogramming of host cells in response to enteroviral infection," *Cells*, vol. 9, no. 2, p. 473, 2020.

[43] M. Ogawa, Y. Shirasago, I. Tanida et al., "Structural basis of antiviral activity of caffeic acid against severe fever with thrombocytopenia syndrome virus," *Journal of Infection and Chemotherapy*, vol. 27, no. 2, pp. 397–400, 2021.

[44] J. M. Hare, F. Beigi, and K. Tziomalos, "Nitric oxide and cardiobiology-methods for intact hearts and isolated myocytes," in *Methods in Enzymology*, pp. 369–392, Elsevier, 2008.

[45] R. Dringen, "Neuron–glia coupling in glutathione metabolism," in *Encyclopedia of Neuroscience*, pp. 733–737, Elsevier, 2009.

[46] G. Wu, C. J. Meininger, C. J. McNeal, F. W. Bazer, and J. M. Rhoads, "Role of L-arginine in nitric oxide synthesis and health in humans," in *Amino Acids in Nutrition and Health*, vol. 1332 of Advances in Experimental Medicine and Biology, , pp. 167–187, Springer, Cham, 2021.

[47] M. Norval, T. J. Simpson, and J. A. Ross, "Urocanic acid and immunosuppression," *Photochemistry and Photobiology*, vol. 50, no. 2, pp. 267–275, 1989.

[48] J. J. Finlay-Jones and P. H. Hart, "Ultraviolet irradiation, systmic immunosuppression and skin cancer: role of urocanic acid," *The Australasian Journal of Dermatology*, vol. 38, Supplement 1, pp. S7–12, 1997.